CrossMark

J. Plasma Phys. (2022), *vol*. 88, 895880601 © The Author(s), 2022.
Published by Cambridge University Press
doi:10.1017/S0022377822001179

Nonlinear excitation of geodesic acoustic mode by reversed shear Alfvén eigenmodes in non-uniform plasmas

Y. Wang[1], N. Chen[1], T. Wang[1,2], S. Wei[1] and Z. Qiu[1,2,†]

[1]Institute for Fusion Theory and Simulation and School of Physics, Zhejiang University, Hangzhou 310027, PR China

[2]Center for Nonlinear Plasma Science and ENEA C R Frascati, 00044 Frascati, Italy

(Received 6 July 2022; revised 30 October 2022; accepted 1 November 2022)

Effects of plasma non-uniformities and kinetic dispersiveness on the spontaneous excitation of geodesic acoustic mode (GAM) by reversed shear Alfvén eigenmode (RSAE) are investigated numerically. It is found that, due to the turning points induced by the shear Alfvén continuum structure, the nonlinear excitation of GAM is a quasiexponentially growing absolute instability. As the radial dependence of GAM frequency and pump RSAE mode structure are accounted for, the radially inward propagating GAM is preferentially excited, leading to core localized thermal plasma heating by GAM collisionless damping. Our work, thus, suggests that GAM excitation plays a crucial role in not only RSAE nonlinear saturation, but also anomalous fuel ion heating in future reactors.

Key words: plasma nonlinear phenomena, fusion plasma, plasma instabilities

1. Introduction

Good confinement of energetic particles (EP) including fusion alpha particles is crucial to improve the burning plasma performance and reduce the wall loading of plasma facing materials in the next generation magnetic confinement fusion devices, such as ITER and CFETR (Tomabechi *et al.* 1991; Fasoli *et al.* 2007; Ding *et al.* 2015; Chen & Zonca 2016; Wan *et al.* 2017). Shear Alfvén wave (SAW) instabilities, including Alfvén eigenmodes (Cheng, Chen & Chance 1985) (AEs) and EP continuum modes (Chen 1994), can be resonantly excited by the expansion free energy associated with the non-uniform EP distribution, since EPs have similar characteristic frequencies as those of SAW in typical reactor parameter regimes (Fasoli *et al.* 2007). Even finite amplitude SAW instabilities may cause significant anomalous EP loss and performance degradation (Zonca *et al.* 2015; Chen & Zonca 2016), it is, thus, necessary to have in-depth understanding of the spectrum of SAW, which depends crucially on the nonlinear dynamics of SAW.

There are two possible routes for the nonlinear evolution of EP-driven SAW instability: nonlinear wave–particle phase space dynamics (Berk & Breizman 1990; Todo *et al.* 1995; Zhu, Fu & Ma 2013; Zonca *et al.* 2015; Wang *et al.* 2019) and nonlinear wave–wave

† Email address for correspondence: zqiu@zju.edu.cn

https://doi.org/10.1017/S0022377822001179 Published online by Cambridge University Press

interactions (Sagdeev & Galeev 1969; Hahm & Chen 1995; Chen & Zonca 2013), among which, three-wave parametric decay instability is one of the most fundamental nonlinear wave–wave interactions (Sagdeev & Galeev 1969). Considering the optimal steady state operation scenario of reactors with full non-inductive current drive (Huang *et al.* 2020), as a specific branch of SAW, the reversed shear Alfvén eigenmode (RSAE) (an alternative name is Alfvén cascades) exists close to the flux surface of $q_{\min}$ (Berk *et al.* 2001), and can be preferentially excited by fusion produced alpha particles in the core plasmas (Wang *et al.* 2018). Here, $q_{\min}$ is the off-axis minimum of the safety factor q. Thus, the investigation of the parametric decay process of RSAE has a significant implication for EP transport and overall performance of burning plasmas.

The excitation of geodesic acoustic mode (GAM) (Winsor, Johnson & Dawson 1968; Zonca & Chen 2008; Qiu, Chen & Zonca 2018*a*; Conway, Smolyakov & Ido 2022) by RSAE has been investigated analytically using nonlinear gyrokinetic theory (Wang *et al.* 2022), where a pump RSAE spontaneously decays into a GAM with toroidally symmetric and poloidally near symmetric mode structures, and a daughter kinetic RSAE (KRSAE) with the same toroidal and poloidal mode numbers as those of the pump RSAE, with the frequency and wavevector matching condition satisfied. It is found that, the resonant parametric decay process can occur if the pump RSAE drive can overcome the threshold due to KRSAE and GAM dissipation caused by, e.g. electron and ion Landau damping, respectively. The excited GAM can transfer energy to thermal ions by ion Landau damping. Thus, the investigated process, besides its apparent effects on RSAE nonlinear saturation, also provides a route to collisionless fuel ion heating, i.e. alpha channelling (Fisch & Herrmann 1994; Qiu *et al.* 2018*b*). Note that, for a given q-profile, RSAE frequency lies between toroidal Alfvén eigenmode (TAE) (Cheng *et al.* 1985) and beta-induced Alfvén eigenmode (Heidbrink *et al.* 1993) frequency range, depending on the respective $|nq_{\min} - m|$ value. The present channel, is more effective for RSAEs in the TAE frequency range, to have the frequency and (radial) wavenumber matching conditions satisfied. Here, n/m are the toroidal/poloidal mode numbers of the torus.

Since RSAE is radially localized around the SAW continuum accumulation point induced by the reversed shear magnetic configuration, with the eigenmode structure and frequency determined by plasma non-uniformities, it is natural to expect that, the plasma non-uniformities will also affect the RSAE nonlinear processes, such as the excitation of GAM of interest here. Consistent with the system non-uniformities, the kinetic dispersiveness that determines the radial propagation of both GAM and KRSAE, leading to the GAM/KRSAE sampling of the non-uniformity, may also be important in the nonlinear process (Rosenbluth 1972), and determine the power deposition by Landau damping of the excited sidebands, that may have a direct consequence on the performance of the burning plasmas. This motivates the present study on the system non-uniformity on the nonlinear excitation of GAM by RSAE.

The rest of the paper is organized as follows. In § 2, the model equations describing the parametric decay process of the pump RSAE into a GAM and a KRSAE are given. In § 3, the effects of kinetic dispersiveness on the parametric decay process are investigated. It is found that, when finite group velocities of both GAM and KRSAE are taken into account, the parametric decay process is a convective instability for typical tokamak parameters. In § 4, the effects of non-uniformities, including non-uniform KRSAE and GAM continuum frequencies and the finite radial extent of pump RSAE, on the parametric decay process are investigated. It is found that, the non-uniformity of KRSAE continuum frequency, $\omega_K(r)$, plays a dominant role in rendering the parametric decay process into a quasiexponentially growing absolute instability by trapping the coupled KRSAE and GAM wave packets between the turning points induced by the non-uniformity of $\omega_K(r)$.

https://doi.org/10.1017/S0022377822001179 Published online by Cambridge University Press

The GAM continuum, on the other hand, contributes on the time scale comparable to or shorter than the trapping time due to the non-uniformity of $\omega_K(r)$, and quantitatively modifies the GAM excitation process. Finally, summary and discussions are given in § 5.

2. Theoretical model

In this work, we will investigate the linear growth stage of the excitation of GAM by the pump RSAE, with emphases on the effects of plasma non-uniformities, such as non-uniform KRSAE and GAM continuum frequencies and the finite spatial extent of the pump RSAE (which is also determined by the RSAE continuum), on the parametric decay process. By 'linear growth stage', we mean the feedback of GAM and KRSAE onto the pump RSAE are systematically neglected, which, can become important as the sidebands amplitudes become comparable to the pump RSAE amplitude, and lead to, potentially, complex nonlinear dynamics (Wei, Chen & Qiu 2022) as well as ballistic mode propagation in the form of solitons (Guo, Chen & Zonca 2009; Chen & Zonca 2016; Chen *et al.* 2022). These effects, however, are beyond the scope of present work and focus on the effects of system non-uniformity, and will be investigated in the future.

Since the involved wave frequencies are much smaller than those of the compressional Alfvén wave and $\beta \ll 1$ is considered, the scalar potential $\delta\phi$ and parallel component of vector potential $\delta A_\parallel$ are taken as the field variables for investigating the parametric decay process of the pump RSAE ($\boldsymbol{\Omega}_0 \equiv (\omega_0, \boldsymbol{k}_0)$) into a GAM ($\boldsymbol{\Omega}_G \equiv (\omega_G, \boldsymbol{k}_G)$) and a KRSAE ($\boldsymbol{\Omega}_K \equiv (\omega_K, \boldsymbol{k}_K)$), with β being the ratio of plasma thermal to magnetic pressure. It is convenient to define $\delta\psi = \omega\delta A_\parallel/(ck_\parallel)$ as an alternative field variable for RSAE and KRSAE, where the ideal MHD limit, i.e. vanishing parallel electric field, can be recovered by taking $\delta\psi = \delta\phi$ (Chen & Hasegawa 1991). The total scalar potential perturbation contains $\delta\phi = \delta\phi_0 + \delta\phi_K + \delta\phi_G$, with the subscripts 0, K and G denoting the pump RSAE, KRSAE and GAM, respectively. Considering single-n RSAE/KRSAE with one dominant poloidal model number m, the perturbations of RSAE, KRSAE and GAM in straight-field-line (r, ϑ, φ) flux coordinate can be expressed as

$$\delta\phi_0 = \phi_0 \exp(\mathrm{i}(n\varphi - m\vartheta - \omega_0 t)) + \text{c.c.}, \tag{2.1}$$

$$\delta\phi_K = \phi_K \exp(\mathrm{i}(n\varphi - m\vartheta - \omega_0 t)) \exp\left(-\mathrm{i}\left(\int \hat{k}_G \,\mathrm{d}r - \omega_G t\right)\right) + \text{c.c.}, \tag{2.2}$$

$$\delta\phi_G = \phi_G \exp\left(\mathrm{i}\left(\int \hat{k}_G \,\mathrm{d}r - \omega_G t\right)\right) + \text{c.c.}. \tag{2.3}$$

Here, ϕ is the amplitude of the mode, $\hat{k}_G$ is the radial envelope due to GAM modulation. We note that, the frequency and wavenumber matching conditions, $\boldsymbol{\Omega}_0 = \boldsymbol{\Omega}_K + \boldsymbol{\Omega}_G$, are applied implicitly.

The coupled GAM and KRSAE nonlinear equations can be derived by substituting the non-adiabatic particle responses into the field equations of GAM and KRSAE determined by nonlinear gyrokinetic vorticity equation (Chen & Hasegawa 1991) and charge quasineutrality condition, as

$$\mathcal{E}_{K^*}\delta\phi_{K^*} = -\mathrm{i}\frac{ck_{0,\vartheta}k_G}{B_0\omega_K}A_K\delta\phi_G\delta\phi_{0^*}, \tag{2.4}$$

$$\mathcal{E}_G\delta\phi_G = \mathrm{i}\frac{ck_{0,\vartheta}k_G}{B_0\omega_G}A_G\delta\phi_{K^*}\delta\phi_0, \tag{2.5}$$

while the non-adiabatic particle responses to KRSAE and GAM are derived from the nonlinear gyrokinetic equation (Frieman & Chen 1982). Equations (2.4) and (2.5) are

https://doi.org/10.1017/S0022377822001179 Published online by Cambridge University Press

the nonlinear equations of KRSAE and GAM, respectively. In (2.4), $\mathcal{E}_K \equiv 1 - \Gamma_K - k_{K,\parallel}^2 v_A^2 \sigma_K b_K/\omega_K^2 + \Delta_K$ is the WKB dispersion relation of KRSAE, with $\Gamma_k \equiv \langle \mathrm{J}_k^2 F_0/n_0\rangle$, $v_A = B_0/\sqrt{4\pi n_0 m_i}$ being the Alfvén speed, $\langle\cdots\rangle$ denoting velocity space integration, $\mathrm{J}_k = \mathrm{J}_0(k_\perp \rho_i)$ being the Bessel function of zero index accounting for finite Larmor radius (FLR) effects, ρ_i being the ion Larmor radius, $b_k = k_\perp^2 \rho_i^2/2$, $\sigma_k \equiv \delta\psi_k/\delta\phi_k = 1 + \tau - \tau\Gamma_k$, $\tau = T_e/T_i$, and $\sigma_k \neq 1$ corresponding to deviation from ideal MHD limit due to FLR effects. Furthermore, Δ_K represents the kinetic compression of both thermal and EP, and the KRSAE eigenmode equation can be derived by accounting for the curvature of q at $q_{\min}$. Note that, in the present work focusing on the 'linear growth stage' of the parametric decay process, a finite amplitude pump RSAE is adopted as the initial condition, while its linear excitation by, e.g. EPs, is not considered here. The nonlinear coupling coefficient, $A_K = \Gamma_0 - \Gamma_G - \sigma_0\omega_K(1-\Gamma_K)/(\sigma_K\omega_0)$, contains the contribution from both Reynold stress due to ion nonlinearity as well as finite parallel electric field due to nonlinear electron response to KRSAE. In (2.5), $\mathcal{E}_G \equiv \langle (1-\mathrm{J}_G^2)F_0/n_0\rangle - (T_i/(n_0e^2))\overline{\langle e\omega_d(\mathrm{J}_G\delta H_{G,i}^L - \delta H_{G,e}^L)/\omega_G\rangle}/\overline{\delta\phi_G}$ is the WKB dispersion relation of GAM, with $\overline{(\cdots)} \equiv \int \mathrm{d}\vartheta(\cdots)/(2\pi)$ denoting surface averaging, ω_d being the magnetic drift frequency and δH being the non-adiabatic particle response. The nonlinear coupling coefficient, $A_G \equiv \Gamma_K - \Gamma_0 - (b_0 - b_k)k_\parallel^2 v_A^2 \sigma_0 \sigma_K^*/(\omega_0\omega_K)$, contains the contribution from the nonlinear Reynolds and Maxwell stresses (Chen & Zonca 2012), respectively. Interested readers may refer to Wang *et al.* (2022) for the detailed derivations and the underlying assumptions of (2.4) and (2.5).

Defining $E_G \equiv \partial_r \delta\phi_G$ and adopting the lowest-order KRSAE/GAM dispersion relation, we can obtain the following coupled nonlinear equations:

$$\left[\partial_t(\partial_t + 2\gamma_K) + \omega_K^2 - C_K\omega_K^2\rho_i^2\partial_r^2\right]\delta\hat{\phi}_{K^*} = \partial_t\delta\hat{\phi}_{0^*}E_G, \tag{2.6}$$

$$\left[\partial_t(\partial_t + 2\gamma_G) + \omega_G^2 - C_G\omega_G^2\rho_i^2\partial_r^2\right]E_G = -\partial_t\delta\hat{\phi}_0\partial_r^2\delta\hat{\phi}_{K^*}, \tag{2.7}$$

where $\delta\hat{\phi}_K = \mathrm{i}\sqrt{A_G/A_K}\delta\phi_K$ and $\delta\hat{\phi}_0 = \delta\phi_0\sqrt{A_G A_K}ck_{0,\vartheta}/B_0$ are normalized KRSAE and pump RSAE amplitudes, respectively. The kinetic dispersiveness term of GAM, $\propto C_G$, comes from FLR and finite orbit width effects, and can be obtained from (9) of Qiu, Chen & Zonca (2009). On the other hand, $C_K \simeq 3/4 + \tau$, with terms proportional to $3/4$ and τ represent, respectively, FLR correction to plasma inertial and finite parallel electric field (Chen & Zonca 1995). Here γ_K and γ_G represent the dissipation rates of KRSAE and GAM due to electron and ion contributions to Landau damping, and may determine the threshold of the parametric decay instability. Equations (2.6) and (2.7) are the governing equations describing the parametric decay process of the pump RSAE into the KRSAE and GAM sideband, and will be solved numerically in this work to investigate the effect of plasma non-uniformities as well as kinetic dispersiveness on the nonlinear process. Fourier spectral method for spatial discretization is used in solving (2.6) and (2.7), by changing into a set of ordinary differential equations, which are then solved using MATLAB.

3. The convective/absolute property of the excitation of GAM by RSAE

First, we investigate the effects of finite group velocities due to the kinetic dispersiveness of GAM and KRSAE on the excitation of GAM by a localized pump RSAE. Only the finite radial extent of the pump RSAE, L_P, is taken into account, while the non-uniformities associated with $\omega_K(r)$ and $\omega_G(r)$ are neglected by assuming $L_K = L_G = \infty$, where L_G and L_K are, respectively, the scale length of GAM and KRSAE continuum frequencies. This simplification is valid in that, the pump RSAE radial eigenmode structure is determined by the RSAE continuum structure, and one naturally has $L_K \sim L_G \gg L_P$, and

https://doi.org/10.1017/S0022377822001179 Published online by Cambridge University Press

the effects of $\omega_K(r)$ and $\omega_G(r)$ non-uniformity can be neglected when the considered time scale is shorter than L_K/V_K, i.e. before the wave packet propagates and experience the non-uniformity associated with continuum, with V_K being the characteristic linear KRSAE group velocity, which will be introduced following equation (3.2).

In order to give some insights of the parametric decay process, (2.6) and (2.7) can be reduced to the following form by using temporal and spatial scale expansion of $\delta\hat{\phi}_{K^*}$ and E_G, i.e. $\partial_t \simeq \partial_\eta - \mathrm{i}\omega$, and $\partial_r \simeq \partial_\xi + \mathrm{i}k_r$, with $|\partial_\eta| \ll |\omega|$ and $|\partial_\xi| \ll |k_r|$,

$$(\partial_\eta + \gamma_K + V_K\partial_\xi)\delta\hat{\phi}_{K^*} = \delta\hat{\phi}_{0^*}E_G/2, \tag{3.1}$$

$$(\partial_\eta + \gamma_G + V_G\partial_\xi)E_G = \hat{k}_r^2\delta\hat{\phi}_0\delta\hat{\phi}_{K^*}/2. \tag{3.2}$$

Here $V_G = C_G\omega_G^2\rho_i^2\hat{k}_r/\hat{\omega}$ and $V_K = C_K\omega_K^2\rho_i^2\hat{k}_r/(\hat{\omega}-\omega_0)$, with $\hat{\omega}$ and $\hat{k}_r$ being the frequency and radial wavenumber of GAM determined by the frequency and wavenumber matching conditions of the parametric decay process,

$$(\hat{\omega}-\omega_0)^2 - \omega_K^2 - C_K\omega_K^2\rho_i^2\hat{k}_r^2 = 0, \tag{3.3}$$

$$\hat{\omega}^2 - \omega_G^2 - C_G\omega_G^2\rho_i^2\hat{k}_r^2 = 0. \tag{3.4}$$

If the finite linear group velocities of GAM and KRSAE are neglected, we can obtain the parametric dispersion relation (Wang *et al.* 2022),

$$(\gamma+\gamma_K)(\gamma+\gamma_G) = \frac{\hat{k}_r^2|\delta\hat{\phi}_0|^2}{4}. \tag{3.5}$$

The threshold condition on pump RSAE amplitude for the parametric decay process can be estimated from $\gamma_G\gamma_K = \hat{k}_r^2\delta\hat{\phi}_0^2/4$, i.e. nonlinear drive balances the threshold induced by the KRSAE/GAM dissipations.

When finite group velocities are taken into account, (3.1) and (3.2) are in the standard form of parametric instability discussed in Rosenbluth (1972), and the mode spatiotemporal evolution is given by (14) of Qiu, Chen & Zonca (2014). It is known that the instability is a convective amplification process for $V_KV_G > 0$, i.e. the nonlinearly excited KRSAE and GAM couple together, and propagate away from the initial position with finite group velocity given by $(V_K + V_G)/2$ (Rosenbluth 1972; Qiu *et al.* 2014) and increasing amplitudes as the temporal growth dominates the radial propagation. For $V_KV_G < 0$, on the other hand, the parametric instability is an absolute instability. To show this in detail, (2.6) and (2.7) are solved numerically. Here, the pump RSAE is localized around the region $r_0 = 0$, as shown by the dashed line in figure 1(*a*), while the KRSAE and GAM are initially loaded at r_0 with amplitudes much smaller than that of the pump. The sign of V_KV_G is determined by the sign of C_KC_G for the coupled KRSAE and GAM that satisfy the matching condition, as can be seen from their definitions. The fixed $C_K = 2$ is adopted as a typical parameter, while the sign of C_G can be changed to investigate the absolute/convective property of the parametric decay instability. As shown in figure 1, for $C_G = 1$, GAM and KRSAE are coupled together and propagate out of the pump RSAE localized region in the same direction. The amplitude of GAM at the r_0 decreases with time, exhibiting the typical feature of convective instability. On the other hand, for $C_G = -1$, the amplitude of GAM at r_0 keeps growing exponentially, showing the characteristics of an absolute instability.

Note that, $C_K \simeq 3/4 + \tau$ is positive, while C_G is positive for typical plasma parameters, as discussed in great detail in Zonca & Chen (2008), and $C_G < 0$ is only assumed

https://doi.org/10.1017/S0022377822001179 Published online by Cambridge University Press

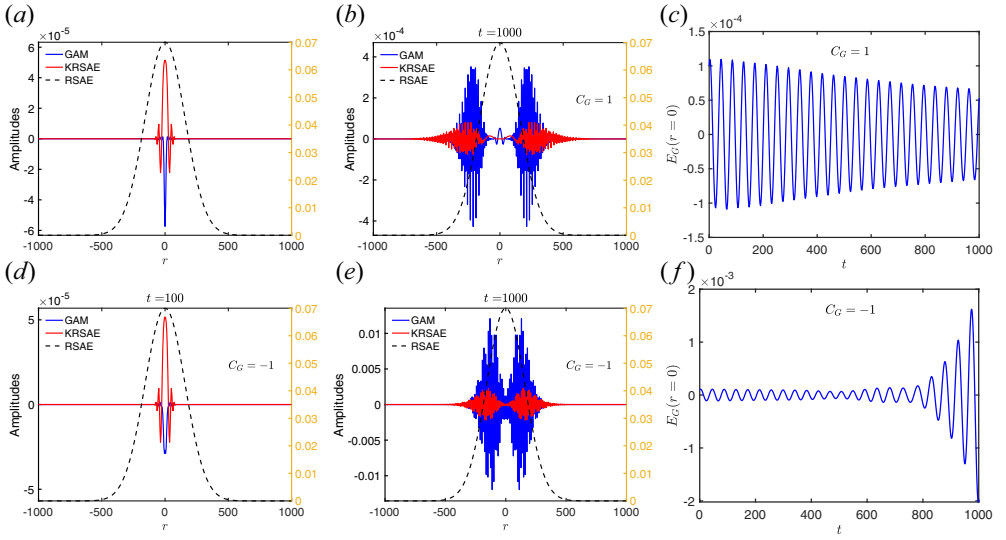

FIGURE 1. The snapshot of mode structures for $C_G = 1$ (a,b), and $C_G = -1$ (d,e). The GAM amplitude at r_0 versus time for $C_G = 1$ (c) and $C_G = -1$ (f). The amplitudes of GAM and KRSAE are on the left-hand y-axis, the amplitude of RSAE on the right-hand y-axis for (a,b,d,e).

artificially here to demonstrate the absolute/convective property of the nonlinear process. Thus, for typical tokamak parameters, the local parametric decay process of the pump RSAE into a GAM and a KRSAE is a convective instability. The generated KRSAE and GAM couple together and propagate out of the unstable region before they can reach sufficiently large amplitude to effectively regulate/suppress Alfvén turbulence. Thus, this process appears to have less interest for improving global confinement performance, which motivates the present investigation of the non-uniform effects associated with GAM and KRSAE continua.

4. Absolute instability of parametric decay process in non-uniform plasma

When spatial scales $|r - r_0| \simeq L_G, L_K$ are considered, the non-uniformity of $\omega_K(r)$, $\omega_G(r)$ and the spatial extent of the pump RSAE must all be taken into account. In particular, the spatial variation of magnetic shear, which correlates with the non-uniform SAW continuum, is mandatory for RSAE formation in realistic tokamak scenario. As will be shown in the following subsections, we construct a representative $\omega_K(r)$ continuum profile as shown in figure 2(a), which is typical for the reversed magnetic shear region, and discuss four scenarios with different combinations of uniform versus non-uniform $\omega_G(r)$ profile and radial structure of the pump RSAE. In all the following numerical cases, as shown in figure 2(a), $\omega_K(r)$ is symmetric about the origin r_0 which corresponds to the SAW continuum accumulational point induced by reversed magnetic shear, $\omega_0 = 0.8\omega_{K0}$, with ω_{K0} being the KRSAE continuum accumulation frequency at r_0, $C_G = 1$ and $C_K = 2$ are adopted in all the following cases.[1] Meanwhile, $\omega_G(r)$ profile and the pump RSAE structure $\delta\hat{\phi}_0$ are shown in figure 2(b,c), respectively, where the solid curves therein

[1]We note that, the RSAE frequency shift from local continuum accumulational point, as a result of local 'q' curvature, i.e. '$\partial^2 q/\partial r^2$', is not included in (2.6), we adopt the 'unrealistic' $\omega_0 = 0.8\omega_{K0}$ to have the KRSAE in the continuum, to capture the main physics that determines the KRSAE power deposition, i.e. the global properties experienced by KRSAE as KRSAE radially propagates.

https://doi.org/10.1017/S0022377822001179 Published online by Cambridge University Press

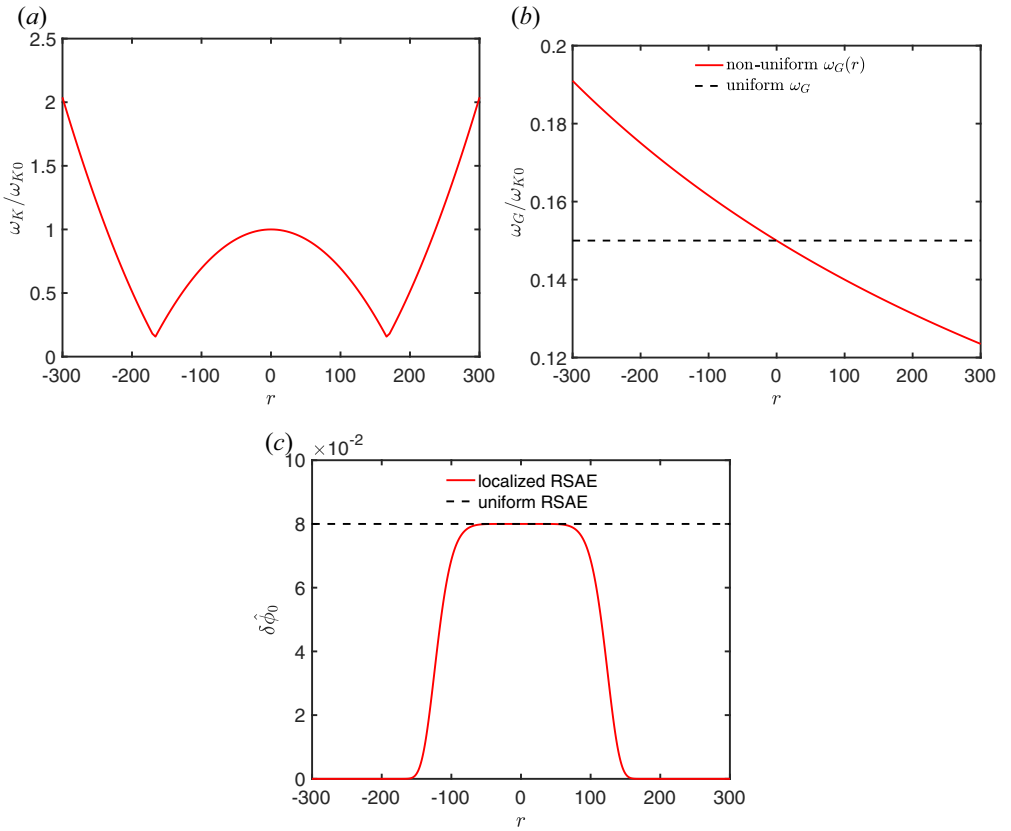

FIGURE 2. The continua of KRSAE (*a*) and GAM (*b*). The normalized mode structure of the pump RSAE (*c*).

correspond to the 'non-uniform case' discussed below and the dashed lines refer to the 'uniform case'.

4.1. *Uniform ω_G and uniform pump RSAE*

In this subsection we investigate the effect of the non-uniform $\omega_K(r)$ on the parametric decay process, neglecting the non-uniformity of $\omega_G(r)$ and the spatial structure of the pump RSAE amplitude. The key parameters include $\omega_G = 0.15\omega_{K0}$ as shown by the dashed line in figure 2(*b*), and a uniform amplitude pump RSAE as shown by the dashed line in figure 2(*c*), and the small KRSAE and GAM initial perturbations are located at r_0, as shown in figure 3(*a*). The KRSAE frequency satisfy the matching condition, and is given by $\omega_K = \omega_0 + \omega_G = 0.95\omega_{K0}$. As can be estimated from figure 2(*a*), ω_K intersects with the KRSAE continuum at $r \simeq \pm 240$, forming a pair of turning points, as shown by the vertical dashed lines in figure 3.

The coupled nonlinear equations (2.6) and (2.7) with the above given parameters are solved numerically as an initial value problem, and the obtained mode structures of KRSAE and GAM at six different times are shown in figure 3. It is found that, the coupled GAM and KRSAE wave packets propagate away from the original position. As the coupled KRSAE/GAM reaches the turning points by KRSAE continuum, majority of propagating wave energy will be bounced back, and then propagate inward, reach the turning points

https://doi.org/10.1017/S0022377822001179 Published online by Cambridge University Press

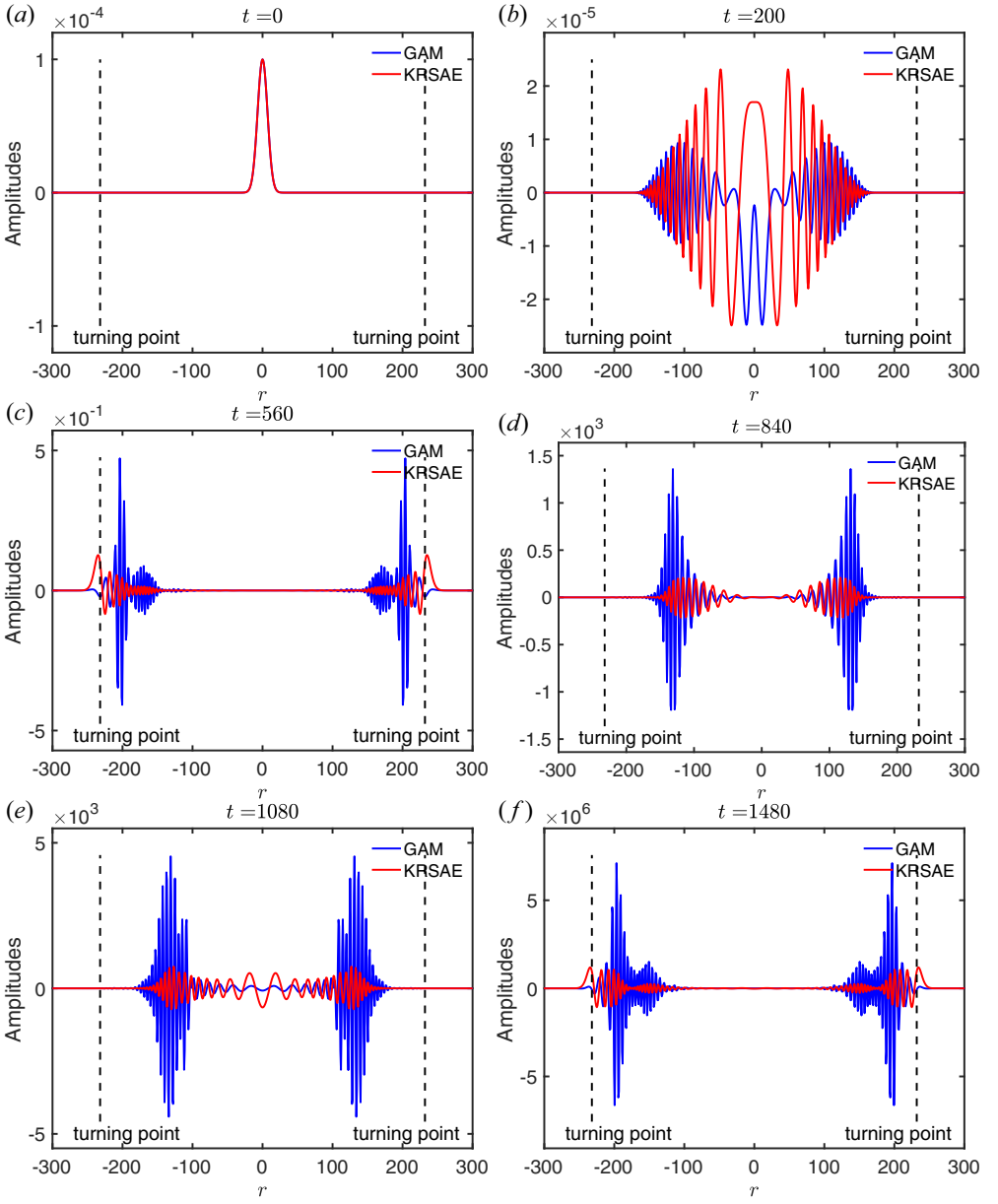

FIGURE 3. Snapshots of mode structures of GAM and KRSAE at six different times with a uniform pump RSAE.

on the other side, completing a full 'bouncing period' of wave packets. Thus, the wave packets are effectively trapped by non-uniform $\omega_K(r)$ structure.

The logarithm of the GAM amplitude at r_0 is shown by the solid curve in figure 4. The amplitude of GAM at r_0 firstly decays in time interval of 0–600, indicating the parametric decay process is indeed a convective instability during this time interval, as shown in § 3. Then the amplitude of GAM at r_0 increases quasiexponentially, after the wave packet is reflected by the turning points, demonstrating that the non-uniform $\omega_K(r)$ structure

https://doi.org/10.1017/S0022377822001179 Published online by Cambridge University Press

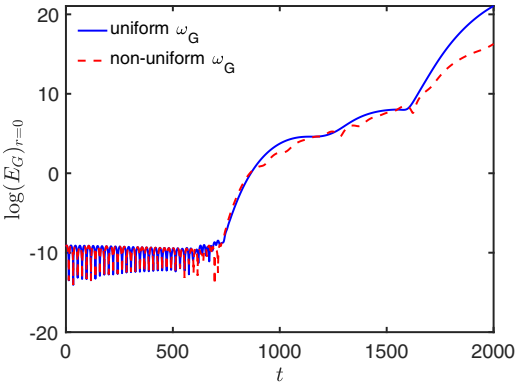

FIGURE 4. Logarithm of E_G versus t with a uniform pump RSAE. The solid curve represents the result with uniform ω_G, while the dashed curve represents the result with non-uniform $\omega_G(r)$.

renders the convective instability into a quasiexponentially growing absolute instability in the longer time scale.

4.2. *Uniform ω_G with localized pump RSAE*

In order to investigate the effect of the finite spatial extent of RSAE on the parametric decay process, the coupled equations (2.6) and (2.7) are solved numerically with a uniform ω_G and a localized pump RSAE, while other parameters are the same as those adopted in § 4.1.

The evolution of GAM and KRSAE mode structures are shown in figure 5. Firstly, the coupled wave packet propagates away from the origin. When the coupled wave packet propagates out of the pump RSAE localized region, GAM and KRSAE are decoupled from each other, as can be clearly seen from (2.6) and (2.7) by turning off the nonlinear coupling due to finite pump amplitude. As a result, KRSAE and GAM mode packets separate in regions with vanishing pump RSAE amplitude, as KRSAE linear group velocity is much larger than that of GAM, as can be seen in figure 5(*b*). When KRSAE reaches the turning points due to non-uniform $\omega_K(r)$, KRSAE will be reflected, and couple with GAM again as the KRSAE reaches the pump RSAE localization region. The coupled KRSAE and GAM wave packets will propagate towards and through the origin with increasing amplitude, until they will decouple again when they propagate away the pump RSAE localized region on the other side. The KRSAE with larger linear group velocity will reach and be reflected by the turning point caused by non-uniform $\omega_K(r)$ on the other side, completing a full bounce period due to non-uniform $\omega_K(r)$, similar to the case shown in § 4.1. We note that GAM, with the linear group velocity much smaller than KRSAE, even though it can propagate outside of the pump RSAE localization region ($r \sim \pm 150$ in figure 5), it will be heavily damped before reaching the turning points, as a finite damping is present, depositing majority of its energy in the tokamak centre.

The amplitude of GAM at r_0 is shown by the solid line in figure 6. It is shown that, the amplitude of GAM at r_0 decreases in the time interval of 0–1800, and grows exponentially after the wave packet is reflected by the turning points, similar to the case with uniform pump RSAE amplitude, as shown by the solid curve in figure 4. By comparing the solid lines in figure 6 with those in figure 4, we can conclude that, while the non-uniform $\omega_K(r)$ plays a dominant role in rendering the parametric decay process into a quasiexponentially growing absolute instability, the overall growth rate of GAM in the case with localized pump RSAE is significantly lower than that with uniform pump RSAE, suggesting the

https://doi.org/10.1017/S0022377822001179 Published online by Cambridge University Press

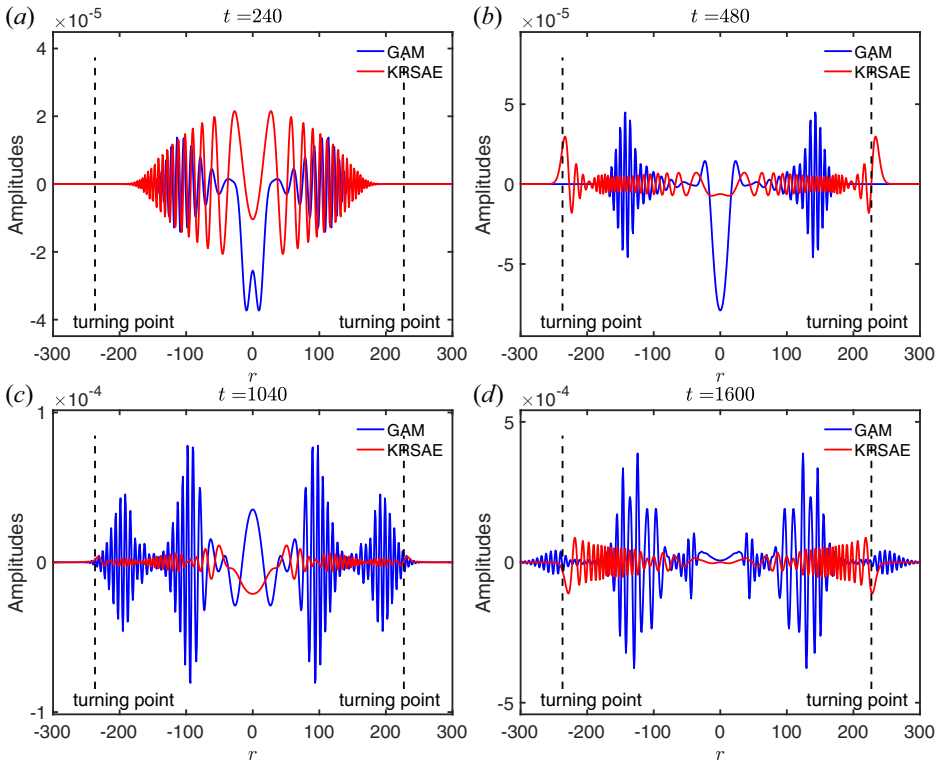

FIGURE 5. Snapshots of mode structures of GAM and KRSAE at four different times with a localized pump RSAE.

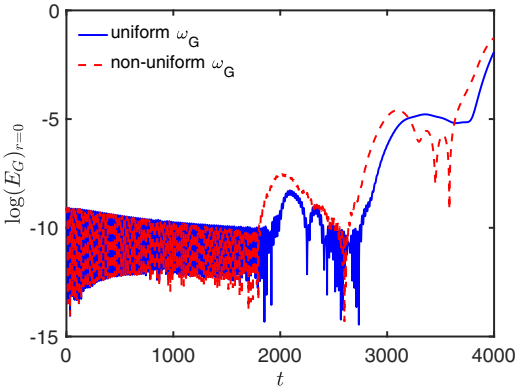

FIGURE 6. Logarithm of E_G versus t with a localized pump RSAE. The solid curves represent the results with uniform $\omega_G(r)$, while the dashed curves represent the results with non-uniform ω_G.

importance of system non-uniformity in qualitatively and quantitatively understanding the GAM excitation in the long time scales.

4.3. *Non-uniform ω_G and uniform pump RSAE*

In order to investigate the effect of non-uniform $\omega_G(r)$ on the parametric decay process, a case similar to that adopted in § 4.1 but with non-uniform $\omega_G(r)$, as shown by the solid line

https://doi.org/10.1017/S0022377822001179 Published online by Cambridge University Press

in figure 2(*b*), is carried out. Due to the non-uniformity of $\omega_G(r)$, one readily finds that the excited GAM has a larger frequency and k_r in the region $r < 0$ than that in the region $r > 0$, which may cause larger growth rate of GAM and KRSAE in the region $r < 0$, as indicated by (3.5).

The obtained mode structures of GAM and KRSAE at six different times are shown in figure 7. It shows that, as anticipated, the mode structures propagating on both sides are not symmetric due to the non-uniformity of $\omega_G(r)$. The wave packet initially propagating towards the $r < 0$ region has larger k_r and, consequently, larger growth rate, as shown in figure 7(*b*). Due to larger group velocity, KRSAE in the region $r < 0$ reaches the turning point earlier than that in the region $r > 0$. Note that, as the wave approaches the turning point, $k_r \to 0$ and thus the KRSAE/GAM growth rate $\gamma \to 0$ consequently, and the wave amplitude on the $r > 0$ sideband may outgrow that on the $r < 0$ side as shown in figure 7(*d*), due to the larger initial group velocity on the $r < 0$ side. Also consistent with the larger initial k_r, the wave packet is firstly reflected by the turning point on the $r < 0$ side, as shown in figure 7(*e*,*f*). Except for the asymmetry induced by $\omega_G(r)$, the evolution of the mode structures of GAM and KRSAE is similar to that described in § 4.1, i.e. the wave packet is trapped between the turning points due to non-uniform $\omega_K(r)$.

The logarithm of GAM amplitude at r_0 is shown by the dashed line in figure 4. It shows that GAM amplitude at r_0 evolves similarly with that in uniform ω_G case, suggesting that $\omega_K(r)$ plays a dominate role on rendering the convective instability into a quasiexponentially absolute instability, while the non-uniform ω_G plays a relatively minor role on quantitatively changing the profile to be asymmetric between the two sides of r_0.

4.4. *Non-uniform ω_G and localized pump RSAE*

In real physical processes, non-uniformities of $\omega_K(r)$ and $\omega_G(r)$ and the finite spatial extent of pump RSAE exist simultaneously. A numerical case containing all the non-uniformities is carried out in this subsection. The pump RSAE is assumed to be localized around r_0 as shown in figure 2(*c*). The non-uniform $\omega_G(r)$ is the solid line shown in figure 2(*b*).

The mode structures of KRSAE and GAM at six different times are shown in figure 8, and the observed phenomena can be understood based on the knowledge obtained from previous cases which delineate each effect separately. Similar to the case in § 4.3, the modes propagating on both sides of r_0 are not symmetric due to larger k_r and consequently, larger growth rate and propagation speed on the $r < 0$ side, as a result of the $\omega_G(r)$ non-uniformity. The major difference with that observed in § 4.3 comes from the localized RSAE pump, which causes the KRSAE and GAM decoupling and stopping growth as they propagate out of RSAE localization. Thus, the vanishing k_r as the KRSAE approaching the turning point, and the resulting longer time of the mode propagating near and reflecting by the turning point, will not cause the mode structure on the $r > 0$ side outgrowing that on $r < 0$ side, as is in the case with uniform pump RSAE. Thus, the mode structure on the $r < 0$ side, always has a much larger amplitude, as shown by figure 8. This may have a direct consequence on RSAE/GAM dissipation induced power deposition to thermal plasmas, noting the anomalous heating rate is typically proportional to the mode intensity. The anomalous thermal ion heating induced by GAM collisionless damping tends to be accumulated in the plasma core region, which may be beneficial for effective power transfer from EP to thermal ions. Finally the evolution of GAM amplitude at r_0 is shown by the dashed curve of figure 6, which is, qualitatively similar to the case with uniform ω_G and localized RSAE pump, confirming the dominant role played by the $\omega_K(r)$ continuum in qualitatively changing the nonlinear process into the quasiexponentially growing absolute instability.

https://doi.org/10.1017/S0022377822001179 Published online by Cambridge University Press

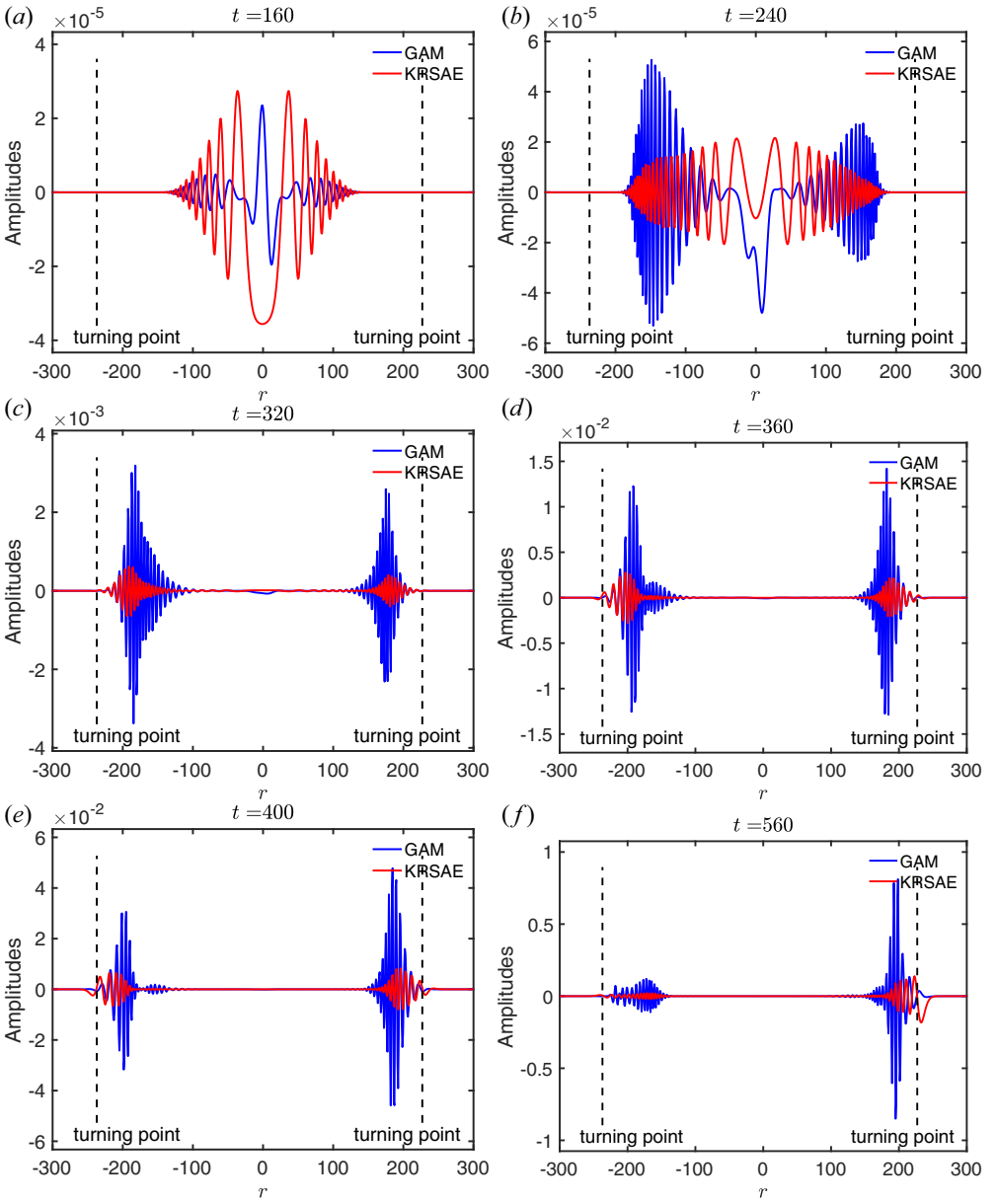

FIGURE 7. Snapshots of mode structures of GAM and KRSAE at six different times with a uniform pump RSAE.

5. Conclusions and discussions

In this paper, nonlinear excitation of GAM by RSAE is investigated numerically in non-uniform plasmas, accounting for the finite linear group velocities of KRSAE and GAM sidebands due to kinetic dispersiveness, non-uniformities of both KRSAE and GAM continuum frequency and finite radial extent of the pump RSAE. This nonlinear decay channel of RSAE was originally proposed and analysed in Wang *et al.* (2022), due to the potential important roles of RSAE nonlinear dynamics in reactor burning plasmas

https://doi.org/10.1017/S0022377822001179 Published online by Cambridge University Press

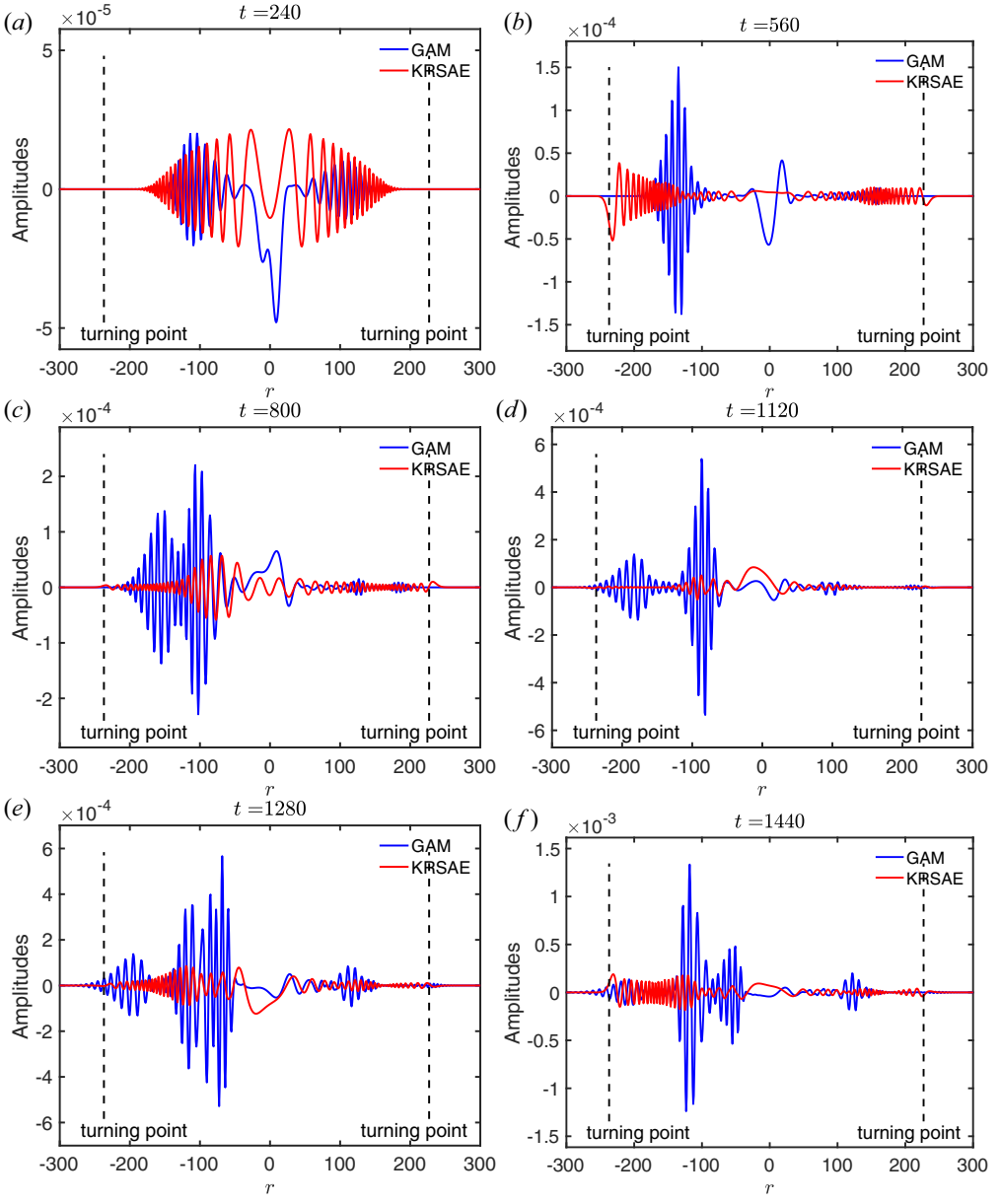

FIGURE 8. Snapshots of mode structures of GAM and KRSAE at six different times with a localized pump RSAE.

with advanced reversed shear configuration and core localized fusion alpha particles. This channel may lead to RSAE nonlinear saturation, as well as thermal plasma heating due to KRSAE/GAM Landau damping, and is expected to directly affect the sustained burning of fusion plasmas. This present investigated process, while very sensitive to plasma parameters, may have a comparable cross-section with other dominant nonlinear mode coupling channels, e.g. zero-frequency zonal structure generation (Wei *et al.* 2021; Wang *et al.* 2022).

https://doi.org/10.1017/S0022377822001179 Published online by Cambridge University Press

For a typical tokamak parameter with C_G and C_K being both positive, the nonlinearly excited GAM and KRSAE satisfying the frequency and wavevector matching conditions propagate radially in the same direction, so the parametric decay of the pump RSAE into a KRSAE and a GAM is a convective amplification process, which motivates the inclusion of system non-uniformity in the analyses. There are three spatial scales involved, L_P, L_G and L_K, corresponding, respectively, to the characteristic scales of pump RSAE width, GAM and SAW continuum variation, and one typically has $L_P \ll L_G \sim L_K$. Since $\omega_K(r)$ is crucial for RSAE existence, it is always kept in the analysis, while cases with different combinations of pump RSAE radial structure and $\omega_G(r)$ non-uniformity are studied to investigate their respective effects on GAM excitaion. It is found that, when the non-uniformity of $\omega_K(r)$ is considered, KRSAE, as well as GAM, will be trapped between the turning points caused by non-uniform $\omega_K(r)$, and the parametric decay process is rendered into a quasiexponentially growing absolute instability. The non-uniformity of $\omega_G(r)$ continuum introduces asymmetries between outward and inward propagating mode amplitudes before the modes reach the turning points induced by the non-uniform $\omega_K(r)$. The radial extent of the pump RSAE can effectively reduce the overall growth rate of the nonlinearly excited GAM. These numerical investigations suggest that kinetic dispersiveness and plasma non-uniformities must be accounted for to correctly capture the property of the parametric decay process and quantitatively assess the power deposition and anomalous plasma heating due to KRSAE and GAM Landau damping. When all the three major non-uniformities as well as kinetic dispersiveness are taken into account, it is found that, the nonlinearly excited KRSAE/GAM have much larger amplitudes in the $r < r_0$ region, which corresponds to a radial inner region with respect to $q_{\min}$. Thus, this nonlinear decay channel of fusion-alpha-particle-driven RSAE, is expected to deposit fusion alpha particle power in the tokamak centre, and directly contributes to the sustained burning of fusion reactors.

In the present study, the KRSAE/GAM sidebands dissipation rates, γ_G and γ_K, are systematically taken as zero, to focus on the global property of the nonlinear process, i.e. the propagation of the coupled KRSAE/GAM wave packets between the two turning points induced by $\omega_K(r)$ continuum. We note that, γ_G and γ_K are crucial for the 'alpha channelling' process, as they not only determine the threshold of the spontaneous decay process, but also determine the rate of thermal plasma heating. In fact, the former requires γ_G and γ_K to be small to have the decay process occur, while the latter, requires γ_G and γ_K to be big to have efficient power transfer to thermal plasmas via GAM/KRSAE Landau damping. Thus, to find the optimized operation regime for efficient collisionless fuel ion heating, more in-depth numerical investigations with realistic geometry are needed, and will be carried out in a future publication.

As a final remark, the present analysis adopts RSAE as a paradigm case, and is general and can be applied to other AEs, e.g. the nonlinear decay of toroidal Alfvén eigenmodes (Cheng *et al.* 1985) into its corresponding kinetic counterpart, kinetic TAE (Mett & Mahajan 1992; Berk, Mett & Lindberg 1993) and GAM (Qiu *et al.* 2018*b*), with the continuum structure consistently changed but the essential physics of distant continuum coupling and wave trapping are the same. The present analysis, however, is of particular importance, as we have addressed, due to the relevance of RSAE in the centre of future reactors (Wang *et al.* 2018; Huang *et al.* 2020).

Acknowledgements

This work is supported by the National Key R&D Program of China under grant nos. 2019YFE03020003 and 2017YFE0301900, the National Science Foundation of China

https://doi.org/10.1017/S0022377822001179 Published online by Cambridge University Press

under grant nos. 11875233 and Users of Excellence program of Hefei Science Center CAS under contract no. 2021HSC-UE016.

Editor P. Catto thanks the referees for their advice in evaluating this article.

Declaration of interests

The authors report no conflict of interest.

REFERENCES

BERK, H.L., BORBA, D.N., BREIZMAN, B.N., PINCHES, S.D. & SHARAPOV, S.E. 2001 Theoretical interpretation of Alfvén cascades in tokamaks with nonmonotonic q profiles. *Phys. Rev. Lett.* **87**, 185002.

BERK, H.L. & BREIZMAN, B.N. 1990 Saturation of a single mode driven by an energetic injected beam. I. Plasma wave problem. *Phys. Fluids* B **2** (9), 2226.

BERK, H.L., METT, R.R. & LINDBERG, D.M. 1993 Arbitrary mode number boundary layer theory for nonideal toroidal Alfvén modes. *Phys. Fluids* B **5** (11), 3969.

CHEN, L. 1994 Theory of magnetohydrodynamic instabilities excited by energetic particles in tokamaks. *Phys. Plasmas* **1** (5), 1519.

CHEN, L. & HASEGAWA, A. 1991 Kinetic theory of geomagnetic pulsations: 1. Internal excitations by energetic particles. *J. Geophys. Res.* **96** (A2), 1503.

CHEN, L. & ZONCA, F. 1995 Theory of shear Alfvén waves in toroidal plasmas. *Phys. Scr.* **1995** (T60), 81.

CHEN, L. & ZONCA, F. 2012 Nonlinear excitations of zonal structures by toroidal Alfvén eigenmodes. *Phys. Rev. Lett.* **109**, 145002.

CHEN, L. & ZONCA, F. 2013 On nonlinear physics of shear Alfvén waves. *Phys. Plasmas* **20** (5), 055402.

CHEN, L. & ZONCA, F. 2016 Alfvén waves and energetic particles. *Rev. Mod. Phys.* **88** (1), 015008.

CHEN, N., WEI, S., WEI, G. & QIU, Z. 2022 Soliton generation and drift wave turbulence spreading via geodesic acoustic mode excitation. *Plasma Phys. Control. Fusion* **64** (1), 015003.

CHENG, C., CHEN, L. & CHANCE, M. 1985 High-n ideal and resistive shear Alfvén waves in tokamaks. *Ann. Phys.* **161**, 21.

CONWAY, G.D., SMOLYAKOV, A.I. & IDO, T. 2022 Geodesic acoustic modes in magnetic confinement devices. *Nucl. Fusion* **62** (1), 013001.

DING, R., PITTS, R., BORODIN, D., CARPENTIER, S., DING, F., GONG, X., GUO, H., KIRSCHNER, A., KOCAN, M., LI, J., *et al.* 2015 Material migration studies with an iter first wall panel proxy on east. *Nucl. Fusion* **55** (2), 023013.

FASOLI, A., GORMENZANO, C., BERK, H., BREIZMAN, B., BRIGUGLIO, S., DARROW, D., GORELENKOV, N., HEIDBRINK, W., JAUN, A., KONOVALOV, S., *et al.* 2007 Chapter 5: physics of energetic ions. *Nucl. Fusion* **47** (6), S264.

FISCH, N. & HERRMANN, M. 1994 Utility of extracting alpha particle energy by waves. *Nucl. Fusion* **34** (12), 1541.

FRIEMAN, E.A. & CHEN, L. 1982 Nonlinear gyrokinetic equations for low-frequency electromagnetic waves in general plasma equilibria. *Phys. Fluids* **25** (3), 502–508.

GUO, Z., CHEN, L. & ZONCA, F. 2009 Radial spreading of drift-wave & zonal-flow turbulence via soliton formation. *Phys. Rev. Lett.* **103**, 055002.

HAHM, T.S. & CHEN, L. 1995 Nonlinear saturation of toroidal Alfvén eigenmodes via ion compton scattering. *Phys. Rev. Lett.* **74**, 266.

HEIDBRINK, W., STRAIT, E., CHU, M. & TURNBULL, A. 1993 Observation of beta-induced Alfvén eigenmodes in the DIII-D tokamak. *Phys. Rev. Lett.* **71** (6), 855.

HUANG, J., GAROFALO, A., QIAN, J., GONG, X., DING, S., VARELA, J., CHEN, J., GUO, W., LI, K., WU, M., *et al.* 2020 Progress in extending high poloidal beta scenarios on DIII-D towards a steady-state fusion reactor and impact of energetic particles. *Nucl. Fusion* **60** (12), 126007.

METT, R.R. & MAHAJAN, S.M. 1992 Kinetic theory of toroidicity-induced Alfvén eigenmodes. *Phys. Fluids* B **4** (9), 2885–2893.

https://doi.org/10.1017/S0022377822001179 Published online by Cambridge University Press

QIU, Z., CHEN, L. & ZONCA, F. 2009 Collisionless damping of short wavelength geodesic acoustic modes. *Plasma Phys. Control. Fusion* **51** (1), 012001.

QIU, Z., CHEN, L. & ZONCA, F. 2014 Excitation of kinetic geodesic acoustic modes by drift waves in nonuniform plasmas. *Phys. Plasmas* **21** (2), 022304.

QIU, Z., CHEN, L. & ZONCA, F. 2018*a* Kinetic theory of geodesic acoustic modes in toroidal plasmas: a brief review. *Plasmas Sci. Technol*. **20** (9), 094004.

QIU, Z., CHEN, L., ZONCA, F. & CHEN, W. 2018*b* Nonlinear decay and plasma heating by a toroidal Alfvén eigenmode. *Phys. Rev. Lett*. **120** (13), 135001.

ROSENBLUTH, M.N. 1972 Parametric instabilities in inhomogeneous media. *Phys. Rev. Lett*. **29**, 565–567.

SAGDEEV, R. & GALEEV, A. 1969 *Nonlinear Plasma Theory*. AW Benjamin Inc.

TODO, Y., SATO, T., WATANABE, K., WATANABE, T. & HORIUCHI, R. 1995 Magnetohydrodynamic vlasov simulation of the toroidal Alfvén eigenmode. *Phys. Plasmas* **2** (7), 2711.

TOMABECHI, K., GILLELAND, J., SOKOLOV, Y., TOSCHI, R. & TEAM, I. 1991 Iter conceptual design. *Nucl. Fusion* **31** (6), 1135.

WAN, Y., LI, J., LIU, Y., WANG, X., CHAN, V., CHEN, C., DUAN, X., FU, P., GAO, X., *et al.* 2017 Overview of the present progress and activities on the CFETR. *Nucl. Fusion* **57** (10), 102009.

WANG, T., QIU, Z., ZONCA, F., BRIGUGLIO, S., FOGACCIA, G., VLAD, G. & WANG, X. 2018 Shear Alfvén fluctuation spectrum in divertor tokamak test facility plasmas. *Phys. Plasmas* **25** (6), 062509.

WANG, T., WANG, X., BRIGUGLIO, S., QIU, Z., VLAD, G. & ZONCA, F. 2019 Nonlinear dynamics of shear Alfvén fluctuations in divertor tokamak test facility plasmas. *Phys. Plasmas* **26** (1), 012504.

WANG, Y., WANG, T., WEI, S. & QIU, Z. 2022 Nonlinear excitation of a geodesic acoustic mode by reversed shear Alfvén eignemodes. *Plasmas Sci. Technol*. **24** (2), 025105.

WEI, G., CHEN, N. & QIU, Z. 2022 Nonlinear interaction of EGAM with DW turbulence in the dimits shift region. *Acta Phys. Sin*. **71** (1), 015201.

WEI, S., WANG, T., CHEN, N. & QIU, Z. 2021 Nonlinear reversed shear Alfvén eigenmode saturation due to spontaneous zonal current generation. *J. Plasma Phys*. **87** (5), 905870505.

WINSOR, N., JOHNSON, J.L. & DAWSON, J.M. 1968 Geodesic acoustic waves in hydromagnetic systems. *Phys. Fluids* **11** (11), 2448–2450.

ZHU, J., FU, G. & MA, Z. 2013 Nonlinear dynamics of toroidal Alfvén eigenmodes driven by energetic particles. *Phys. Plasmas* **20** (7), 072508.

ZONCA, F. & CHEN, L. 2008 Radial structures and nonlinear excitation of geodesic acoustic modes. *Europhys. Lett*. **83** (3), 35001.

ZONCA, F., CHEN, L., BRIGUGLIO, S., FOGACCIA, G., VLAD, G. & WANG, X. 2015 Nonlinear dynamics of phase space zonal structures and energetic particle physics in fusion plasmas. *New J. Phys*. **17** (1), 013052.

https://doi.org/10.1017/S0022377822001179 Published online by Cambridge University Press